Speed and Accuracy in 3D Resistivity Modeling

Spitzer, K.[1]
Niedersächsisches Landesamt für Bodenforschung – Geowissenschaftliche Gemeinschaftsaufgaben, Stilleweg 2, 30655 Hannover, Germany

Wurmstich, B.
Deceased. Formerly Western Atlas Logging Services, 10201 Westheimer Rd., Houston, TX 77042, USA

Abstract

Two main concerns in numerical modeling are accuracy and speed. Accuracy is closely related to the utilized discretization scheme while speed is achieved by using efficient equation solvers. We discuss both topics for elliptic second–order differential equations as they appear in 3D FD resistivity modeling. The first section compares five FD discretization approaches in terms of accuracy. Three discretization schemes yield good results: a method using volume–weighted averages from conductivities assigned to neighboring grid cells, an elemental volume integrating method and a resistivity network approach. The discretization by elemental volume leads to coupling coefficients that are similar to those derived from the volume-weight method. The coefficients only differ by a real factor. In the second section, the cumulative amount of numerical work as a measure of speed is compared for five different equation solvers with and without preconditioning. The most efficient equation solver for symmetric matrices is the preconditioned conjugate gradient method. More general matrix solution methods for both symmetric and non-symmetric matrices such as orthomin, and the methods of stabilized biconjugate gradients and squared conjugate gradients also achieve satisfactory convergence rates.

1 Introduction

Only a few publications study methods of 3D FD resistivity modeling (e.g., Dey & Morrisson 1979b, Scriba 1981). However, 3D finite difference resistivity modeling only becomes practical when the problem can be solved accurately and efficiently at the same time. We address both issues in this paper.

The resistivity problem is governed by second-order elliptic partial differential equations (Poisson's or Laplace's equations) that define a boundary value problem. Different approaches may be used to derive finite difference discretizations of the second-order elliptic partial differential equations. We restrict the discussion to 7–point finite difference discretization schemes that are most commonly used because of their simplicity and relatively conservative storage requirements. For 7–point discretization schemes we discuss possibilities of deriving a linear set of FD equations that approximate the analytical formulation as accurately as possible.

The linear set of FD equations can be expressed in matrix notation, where the coefficient matrix usually is sparse, banded, and diagonally dominant. The matrix may also be symmetric depending on the method of incorporating boundary conditions. Conjugate gradient and conjugate residual methods are among the most efficient generalized equation solvers for finite difference equations since they take advantage of the sparse banded structure of the coefficient matrix. Conjugate gradient/residual methods are guaranteed to converge in the absence of round–off errors, and they are less affected by them than, e.g., LU-decomposition or Gaussian elimination. The cumulative amount of numerical work is used as a hardware-independent measure to evaluate the performance of different equation solvers based on the conjugate gradient and conjugate residual methods. In this context, we also refer to the work of Agarwal & Weaver (1994) dealing with the performance of a variety of equation solvers in conjunction with electromagnetic modeling.

2 Accuracy: Comparison of Five Discretization Schemes

Most 3D FD approaches are derived as 7–point finite difference discretization schemes. The discretization approximates the partial differential equations locally between a center grid point and its six direct neighbors along the main coordinate axes. Electrical conductivity values may be arbitrarily distributed within the halfspace. Variable grid spacing is incorporated in each case.

[1] now at: École Polytechnique, P.O. Box 6079, Succ. Centre-Ville, Montreal, H3C 3A7 Canada

In general, it is possible to formulate FD approaches with more than the six direct neighbors along the main coordinate axes. For example, when all diagonal neighbors of a finite difference grid point are taken into account, a 27–point FD–star is obtained with 27 coupling coefficients (Rodemann 1994). The accuracy should increase especially in directions that are not aligned with the principal axis of the coordinate system, because grid-orientation effects (Rossen & Dalton 1990) can be reduced. However, memory requirements are expanded. Owing to limited computer memory, the number of grid points of the 27–point grid will be smaller and thus accuracy is inevitably decreased. This trade–off is subject to further investigations.

The five 7–point FD approaches are described in the following. In each case, Neumann boundary conditions ($\partial V/\partial z = 0$) are applied at the surface and Dirichlet boundary conditions ($V = 0$) at all other boundaries.

2.1 The Methods

2.1.1 Brewitt-Taylor & Weaver (1976) [BT&W]

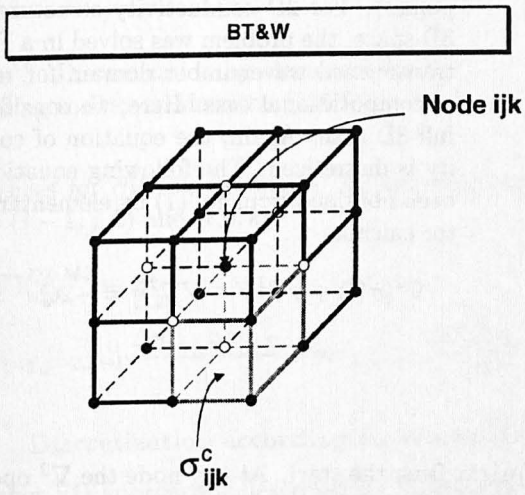

Figure 1: Discretization according to Brewitt-Taylor & Weaver (1976).

This discretization scheme was originally designed for magnetotelluric model calculations by Brewitt-Taylor & Weaver (1976) and was adopted for 2D DC resistivity modeling by Mundry (1984). Spitzer (1995) transcribed this approach into 3D and combined it with efficient preconditioned conjugate gradient type equation solvers.

The governing partial differential equation is the equation of continuity

$$\nabla \cdot (\sigma \nabla V) = Q \qquad (1)$$

with σ as the electric conductivity, V as the electric potential, and Q as the source term. Q is defined by the electric current I and Dirac's delta function δ

$$Q = -I\,\delta(x - x_q)\,\delta(y - y_q)\,\delta(z - z_q) \quad . \qquad (2)$$

As σ is a scalar function of space, it follows that

$$\sigma\left(\frac{\partial^2 V}{\partial x^2} + \frac{\partial^2 V}{\partial y^2} + \frac{\partial^2 V}{\partial z^2}\right) + \frac{\partial \sigma}{\partial x}\frac{\partial V}{\partial x} + \frac{\partial \sigma}{\partial y}\frac{\partial V}{\partial y} + \frac{\partial \sigma}{\partial z}\frac{\partial V}{\partial z} = -I\,\delta(x - x_q)\,\delta(y - y_q)\,\delta(z - z_q) \quad . \qquad (3)$$

The central FD discretization for the potential and its derivatives at the nodes is achieved by a second–order Taylor series expansion. Conductivities $\sigma_{i,j,k}$ at the grid points are calculated by a volume–weighted arithmetic average from conductivities assigned to grid cells $\sigma^c_{i,j,k}$. FD expressions for the conductivity gradients $\partial\sigma/\partial x$, $\partial\sigma/\partial y$, $\partial\sigma/\partial z$ are derived analogously. The source term is discretized through a finite source volume

$$\tau = \frac{(\Delta x_{i_q-1} + \Delta x_{i_q})(\Delta y_{j_q-1} + \Delta y_{j_q})\Delta z_1}{8} \qquad (4)$$

for the special case of a source at the surface, yielding

$$Q \approx -\frac{I}{\tau} \quad . \qquad (5)$$

i_q, j_q and 1 are the source indices and Δx_i, Δy_j, and Δz_k are the grid spacings in x–, y–, and z–direction, respectively. The discretized FD formulation of eq. (3) is

$$C1_{i,j,k}V_{i-1,j,k} + C2_{i,j,k}V_{i+1,j,k} + C3_{i,j,k}V_{i,j-1,k} + C4_{i,j,k}V_{i,j+1,k} + C5_{i,j,k}V_{i,j,k-1} + C6_{i,j,k}V_{i,j,k+1}$$
$$= C0_{i,j,k}V_{i,j,k} - Q \qquad (6)$$

and the resulting coefficients read as follows (only for x–direction and for the nodes $(i-1,j,k)$ and (i,j,k)):

$$C1_{i,j,k}^{BT\&W} = \frac{2\sigma_{i,j,k} - \frac{\partial \sigma_{i,j,k}}{\partial x}\Delta x_i}{\Delta x_{i-1}(\Delta x_{i-1} + \Delta x_i)} \qquad (7)$$

2.1.2 Discretization by points according to Dey & Morrison (1979a) [D&M1]

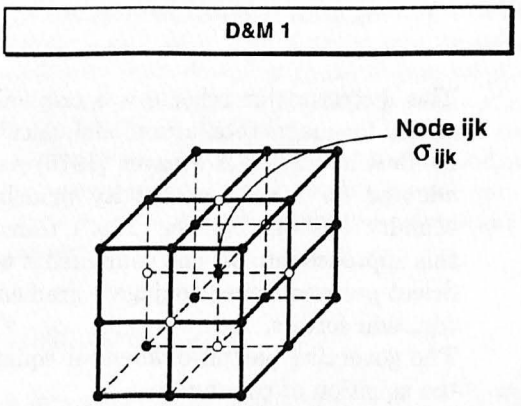

Figure 2: Discretization by points according to Dey & Morrison (1979a).

This method was introduced for 2D resistivity modeling and was labeled as "discretization by points". For 2D conductivity structures in a 3D space, the problem was solved in a Fourier transformed wavenumber domain for reasons of computational ease. Here, we consider the full 3D case. Again, the equation of continuity is discretized. The following equation has been obtained from eq. (1) by elementary vector calculus

$$\nabla^2(\sigma V) + \sigma\nabla^2 V - V\nabla^2\sigma = -2Q \quad . \qquad (8)$$

Conductivities $\sigma_{i,j,k}$ are assigned to the nodes (i,j,k) right from the start. At any node the ∇^2 operator on any distribution $P_{i,j,k}$ is approximated by the following FD equation:

$$\begin{aligned}\nabla^2 P_{i,j,k} \;=\; & \frac{2}{\Delta x_i + \Delta x_{i-1}}\left[\frac{P_{i-1,j,k} - P_{i,j,k}}{\Delta x_{i-1}} + \frac{P_{i+1,j,k} - P_{i,j,k}}{\Delta x_i}\right] \\ & + \frac{2}{\Delta y_j + \Delta y_{j-1}}\left[\frac{P_{i,j-1,k} - P_{i,j,k}}{\Delta y_{j-1}} + \frac{P_{i,j+1,k} - P_{i,j,k}}{\Delta y_j}\right] \\ & + \frac{2}{\Delta z_k + \Delta z_{k-1}}\left[\frac{P_{i,j,k-1} - P_{i,j,k}}{\Delta z_{k-1}} + \frac{P_{i,j,k+1} - P_{i,j,k}}{\Delta z_k}\right] .\end{aligned} \qquad (9)$$

$P_{i,j,k}$ stands for either $V_{i,j,k}$, $\sigma_{i,j,k}$, or $(\sigma_{i,j,k}V_{i,j,k})$. The coupling coefficients are derived as the mean value of the grid point conductivities weighted by the grid spacing (again only for x):

$$C1_{i,j,k}^{D\&M1} = \frac{\sigma_{i-1,j,k} + \sigma_{i,j,k}}{\Delta x_{i-1}(\Delta x_{i-1} + \Delta x_i)} \qquad (10)$$

2.1.3 Discretization by elemental volume according to Dey & Morrison (1979b) [D&M2]

Green's theorem. The integrand of the right side is approximated by I/τ (according to eq. 4 and 5), yielding

$$\iint_{s_{i,j,k}} \sigma \frac{\partial V}{\partial \eta}\, ds_{i,j,k} = -\iiint_{\Delta v_{i,j,k}} I/\tau \, dv_{i,j,k} \quad , \qquad (12)$$

where η is the outward normal. The right-hand side of eq. (12) becomes $-2I$ at the location of the sources. The factor 2 appears because of the halved source volume at the surface. Using central finite

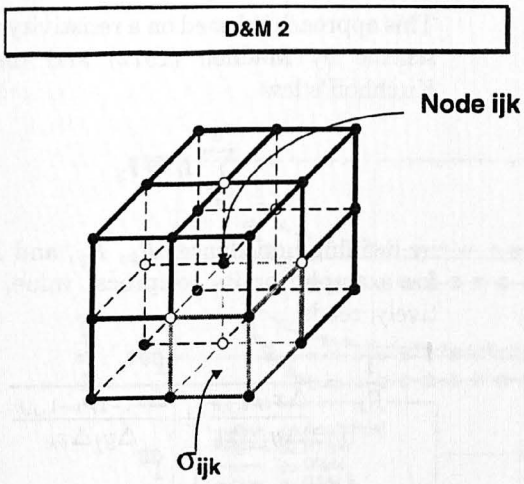

Figure 3: Discretization by elemental volume according to Dey & Morrison (1979b).

Dey & Morrison (1979a) described another FD scheme called "discretization by area", which was taken to be the basis for their 3D approach (Dey & Morrison 1979b) labeled "discretization by elemental volume". Conductivities are assigned to grid cells.
The governing differential equation is the volume integrated form of the equation of continuity [eq. (1)]:

$$\iiint_{\Delta v_{i,j,k}} \nabla \cdot (\sigma \nabla V)\, dv_{i,j,k}$$

$$= -\iiint_{\Delta v_{i,j,k}} I\delta(x-x_q)\delta(y-y_q)\delta(z-z_q)\, dv_{i,j,k} \quad . \tag{11}$$

The volume integral of the left side is converted into a surface integral along the six sides of the elemental volume $\Delta v_{i,j,k}$ using

differences for $\partial V/\partial \eta$, we obtain the following coupling coefficients, again as an example only for the nodes $(i-1,j,k)$ and (i,j,k):

$$C1^{D\&M2}_{i,j,k} = \frac{1}{\Delta x_{i-1}}$$
$$\left(\sigma_{i-1,j-1,k-1}\frac{\Delta y_{j-1}\Delta z_{k-1}}{4} + \sigma_{i-1,j,k-1}\frac{\Delta y_j \Delta z_{k-1}}{4} + \sigma_{i-1,j-1,k}\frac{\Delta y_{j-1}\Delta z_k}{4} + \sigma_{i-1,j,k}\frac{\Delta y_j \Delta z_k}{4}\right) \quad . \tag{13}$$

2.1.4 Discretization according to Wurmstich & Morgan (1994) [W&M]

A further FD approach is described by Wurmstich & Morgan (1994). This approach was adopted from reservoir simulation and is based on a conductivity network, using the principle of conservation of charge. Conductivities are assigned to the grid cells; nodal points are located in the center of each cell. According to Kirchhoff's law, the partial currents $I_l = A_l j_l$, $l = 1,\ldots,6$, are summed up at each node to balance the source current I_S

$$\sum_{l=1}^{6} A_l j_l = I_S \quad . \tag{14}$$

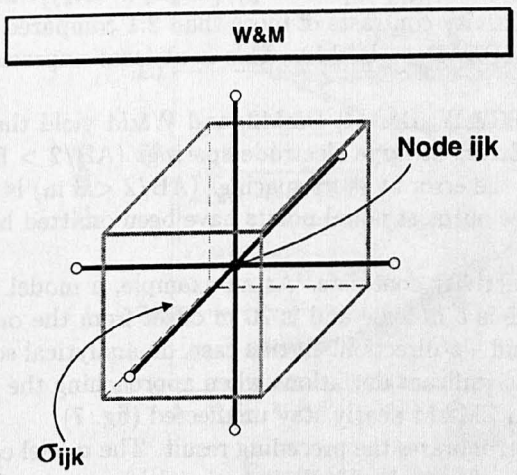

Figure 4: Discretization according to Wurmstich & Morgan (1994).

A_l is the l^{th} face of the grid cell through which the current of the density j_l flows. The conductivity $\overline{\sigma}_{i,j,k}$ between two nodes is calculated by a harmonic mean value of conductivities of neighboring grid cells, here for example in x-direction for node (i,j,k) and $(i+1,j,k)$:

$$\overline{\sigma}_{i,j,k} = 2\,\frac{\sigma_{i,j,k}\sigma_{i+1,j,k}}{\sigma_{i,j,k}+\sigma_{i+1,j,k}} \quad . \tag{15}$$

I_S is only non–zero in those volumes containing sources or sinks. The corresponding coupling coefficient is

$$C1^{W\&M}_{i,j,k} = 4\,\frac{\overline{\sigma}_{i,j,k}}{\Delta x_{i-1}(\Delta x_{i-1}+\Delta x_i)} \tag{16}$$

2.1.5 Discretization according to Zhang et al. (1995) [ZM&M]

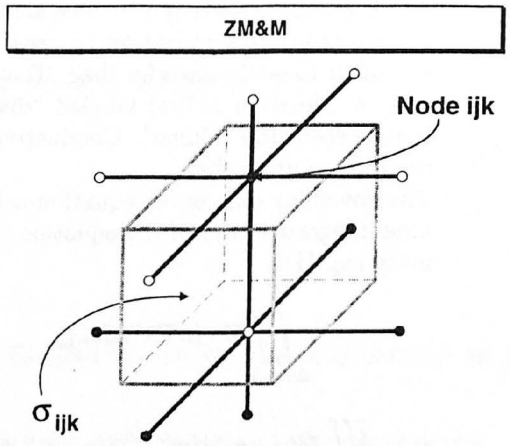

Figure 5: Discretization according to Zhang et al. (1995).

This approach is based on a resistivity network scheme by Madden (1972) and discretizes Kirchhoff's law

$$\sum_{l=1}^{6} I_l = I_S \tag{17}$$

by defining impedances R_x, R_y, and R_z. R_x, for example, or its reciprocal value, respectively, reads

$$\frac{1}{R_x} = \frac{1}{\frac{\Delta x_i \rho_{i,j,k}}{\Delta y_j \Delta z_k} + \frac{\Delta x_{i-1} \rho_{i-1,j,k}}{\Delta y_j \Delta z_k}} + \frac{1}{\frac{\Delta x_i \rho_{i,j,k-1}}{\Delta y_j \Delta z_{k-1}} + \frac{\Delta x_{i-1} \rho_{i-1,j,k-1}}{\Delta y_j \Delta z_{k-1}}}, \tag{18}$$

defining the coupling coefficient $C1_{i,j,k}^{ZM\&M}$. I_S is the resulting source current summing up the six partial currents of each branch along the main axes. Conductivities are assigned to each grid cell; voltage nodes are located at the top and bottom center of each block.

2.2 Results

The accuracy of the five FD discretization schemes is compared for three model classes: 1. the homogeneous halfspace (fig. 6), 2. a dike model (fig. 7), and 3. a three–layered earth (fig. 8). The utilized grid has $63 \times 63 \times 30$ grid lines. The modeling domain boundaries are located at ± 2520 m in x- and y–direction and 2520 m in z–direction. Grid spacings increase by a factor of approximately 1.3 towards the outer boundaries. The two sources are located at (± 1 m, 0 m, 0 m). Because of its special practical concern, the comparison is carried out in terms of apparent resistivities $\rho_a = k\Delta V/I$ with k as the geometrical factor derived from Schlumberger arrangements, I as the source current, and ΔV as the corresponding potential difference. ρ_a, which could also be regarded as a normalised potential, is calculated exploiting the principle of reciprocity and plotted as a function of the half electrode spacing AB/2. In each plot there is a right ordinate indicating the relative deviation to the analytically determined values or, in the case of the three–layered earth, to the results obtained by applying a 1D linear filter method (e.g., Koefoed 1979).

Because the results for BT&W are identical to D&M2, we omit all D&M2 curves in the figures. In fact, it can be shown that the two approaches are equal, when the source terms and the coefficients for BT&W are divided by the elemental volume $8/\big((\Delta x_{i-1} + \Delta x_i)(\Delta y_{j-1} + \Delta y_j)(\Delta z_{k-1} + \Delta z_k)\big)$. Mundry (1984) stated a higher accuracy for BT&W at conductivity contrasts of more than 2:1 compared to the approach of Dey & Morrison (1979a), not specifying D&M1 or D&M2. This is at least unprecise. As shown here, only D&M1 is less accurate than BT&W.

For the homogeneous halfspace of $\rho_1 = 100$ Ωm BT&W, D&M1, D&M2, and W&M yield the same results (fig. 6), while ZM&M yields better results. Errors at large electrode spacings (AB/2 > 800 m) are caused by the boundaries at finite distance, while the error at short spacings (AB/2 < 3 m) is due to the close singularity at the source locations. The three outmost nodal points have been omitted because of the boundary effects.

The accuracy of the methods is affected by conductivity contrasts. As an example, a model with a conductive dike of $\rho_2 = 10$ Ωm is discussed. The dike is 5 m wide and is 20 m offset from the origin of the coordinate system. It extends to infinity in $\pm y$- and $+z$-direction. In this case, an analytical solution exists (Telford et al., 1990). D&M1 and W&M show significant deviations when approaching the lateral conductivity contrasts; whereas, BT&W (D&M2) and ZM&M nearly stay unaffected (fig. 7).

Also the third model class, a stratified medium, corroborates the preceding result. The model consists of three layers. Layer boundaries are at 5 m and 25 m, respectively. The layer resistivities are $\rho_1 = 10$ Ωm,

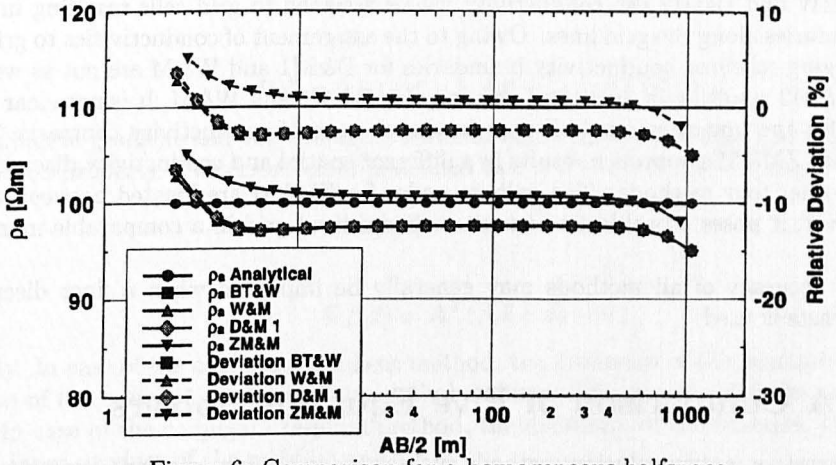

Figure 6: Comparison for a homogeneous halfspace.

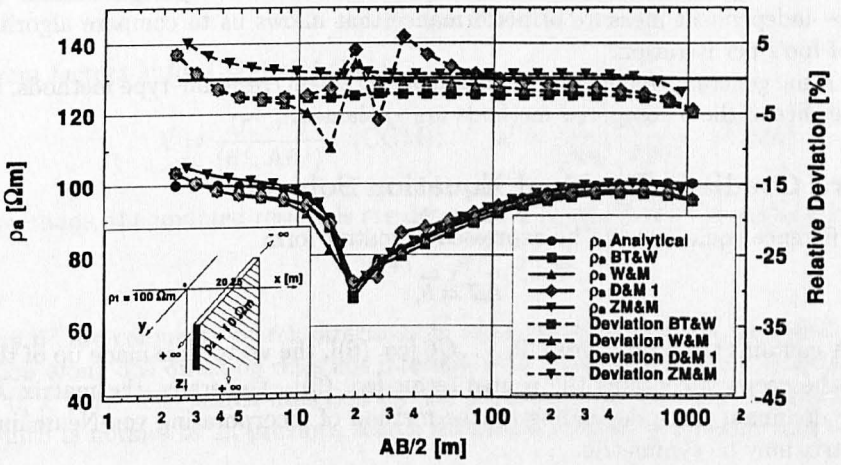

Figure 7: Comparison for a dike model.

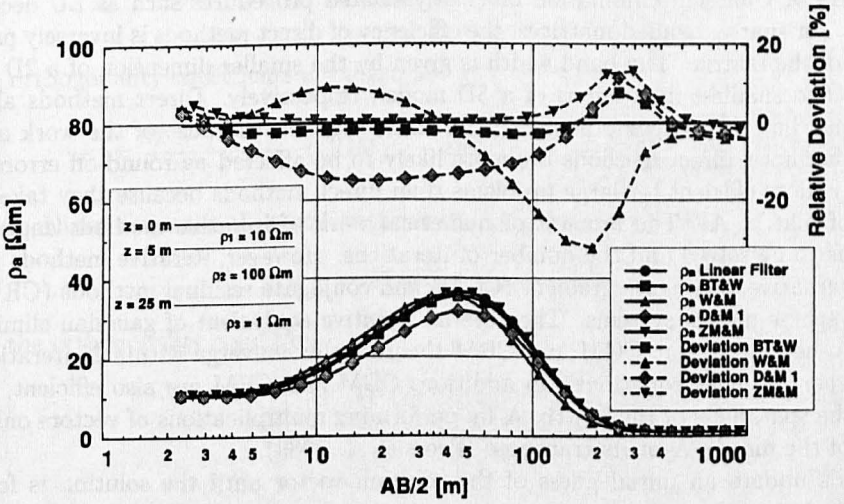

Figure 8: Comparison for a three–layered earth.

$\rho_2 = 100\ \Omega$m, and $\rho_3 = 1\ \Omega$m. Again, more accurate results are obtained for BT&W (D&M2) and ZM&M when layer boundaries are encountered.

The discretization error can be decomposed into a spatial and a conductivity part. The spatial part is the same for BT&W, D&M1, D&M2, and W&M, while the method of discretizing and averaging conductivities differs among the methods. The assignment of conductivities to the grid also differs for all methods. BT&W and D&M2 use conductivity values assigned to grid cells resulting in well defined conductivity boundaries along the grid lines. Owing to the assignment of conductivities to grid points and the selected averaging schemes, conductivity boundaries for D&M1 and W&M are not as well defined as for BT&W and D&M2 resulting in decreased accuracy for D&M1 and W&M. It is not clear why ZM&M is more accurate for the homogeneous halfspace in the absence of conductivity contrasts (fig. 6). One reason could be that ZM&M's approach results in a different spatial and conductivity discretization when compared to the other four methods. The voltage nodes for ZM&M are located between the standard grid nodes. However, it poses a problem to adapt a standardized grid in a comparable manner for each method.

Note that the accuracy of all methods may generally be improved when a finer discretization at conductivity contrasts is used.

3 Speed: A Comparison of Five Equation Solvers

The efficiency of iterative matrix solution methods such as the conjugate gradient–type methods is best expressed in terms of cumulative amount of numerical work. The cumulative work may be defined as floating point operations (fpo) per iteration and grid point. Thus, the cumulative amount of numerical work is a hardware–independent measure of performance that allows us to compare algorithms with a different number of fpo's per iteration.

After outlining some general principles of the conjugate gradient/residual–type methods, and preconditioning, some specifics of the 5 compared methods are explained.

3.1 Conjugate Gradient/Residual Equation Solvers

The set of finite difference equations can be expressed in matrix form

$$\mathbf{A}\vec{x} = \vec{b}, \tag{19}$$

where the matrix $\mathbf{A}$ contains the coefficients $C0, \ldots, C6$ [eq. (6)], the vector $\vec{x}$ is made up of the unknown potentials V, and the vector $\vec{b}$ contains the source terms [eq. (5)]. Generally, the matrix $\mathbf{A}$ is sparse, banded, diagonally dominant, and, depending on the method of incorporating von-Neumann boundary conditions, the matrix may be symmetric.

Methods for solving equation (19) are classified as either direct or iterative methods. Direct methods consist of some form of Gaussian elimination or closely related procedures such as LU decomposition (Press et al. 1989). For sparse, banded matrices, the efficiency of direct methods is inversely proportional to the band width of the matrix. The band width is given by the smaller dimension of a 2D model and the product of the two smallest dimensions of a 3D model, respectively. Direct methods always solve the matrix equations, but they become inefficient for large problems because of the work and storage requirements. Furthermore, direct methods are more likely to be affected by round-off errors. Iterative methods are usually more efficient for large problems than direct methods because they take advantage of the sparseness of matrix $\mathbf{A}$. The amount of numerical work of iterative methods depends on the number of equations to be solved and the number of iterations. However, iterative methods may fail to converge. As an alternative, conjugate gradient (CGM) and conjugate residual methods (CRM) may be used to solve large sparse matrix systems. They are an iterative equivalent of gaussian elimination. In other words, it may be shown that CGM and CRM theoretically converge within N iterations, where N denotes the number of linear equations. In addition, CGM and CRM are also efficient, since they take advantage of the sparseness of the matrix $\mathbf{A}$ by performing multiplications of vectors only with the non-zero elements of the matrix $\mathbf{A}$ or its transpose (Press et al. 1989).

Iterative methods update an initial guess of the solution vector until the solution is found. The iterative process may be written as

$$\mathbf{A}(\vec{x}^{\,l} + \vec{\Delta x}^{\,l+1}) - \vec{b} = \vec{r}^{\,l} - \vec{\Delta r}^{\,l+1}, \tag{20}$$

where l counts the iterations, $\vec{\Delta x}$ and $\vec{\Delta r}$ denote update vectors for $\vec{x}$ and $\vec{r}$, respectively. The initial guess for the solution of eq. (19) is $\vec{x}_0 = 0$ in each investigated case.

Conjugate gradient and conjugate residual methods converge to a minimum of a function $f(\vec{x})$. Choices of $f(\vec{x})$ differ for both methods. The functions to be minimized are (Press et al. 1989)

$$f(\vec{x}) = 0.5\, \vec{x}^T \mathbf{A}\vec{x} - \vec{b}\vec{x} = (\vec{r}, \vec{e})\,, \tag{21}$$

and

$$f(\vec{x}) = 0.5\, (\mathbf{A}\vec{x} - \vec{b}, \mathbf{A}\vec{x} - \vec{b}) = 0.5\, (\vec{r}, \vec{r}) \tag{22}$$

for the conjugate gradient and the conjugate residual method, respectively. The superscript ^{T} indicates the transposed property. The error vector is defined as $\vec{e} = \vec{x} - \vec{x}^{\,l}$. These functions are minimized when

$$\nabla f(\vec{x}) = \mathbf{A}\vec{x} - \vec{b} = 0\,, \tag{23}$$

and

$$\nabla f(\vec{x}) = \mathbf{A}^T(\mathbf{A}\vec{x} - \vec{b}) = 0\,, \tag{24}$$

respectively. In case of the conjugate gradient method, the minimum of the function $f(\vec{x})$ corresponds to the solution of the matrix system which can only be obtained for positive definite and symmetric (PDS) matrices. In case of the conjugate residual method, the minimum of the function $f(\vec{x})$ corresponds to a minimized inner product of the residual vector.

For both, CGM and CRM, the update vector $\vec{\Delta x}^{\,l+1}$ may now be found as the product of the factor λ^l and the vector $\vec{n}^{\,l}$ giving

$$\vec{x}^{\,l+1} = \vec{x}^{\,l} + \lambda^l \vec{n}^{\,l} \tag{25}$$

with different factors λ^l for CGM and CRM

$$\lambda^l = \frac{(\vec{r}^{\,l}, \vec{r}^{\,l})}{(\vec{n}^{\,l}, \mathbf{A}\vec{n}^{\,l})} \quad \text{(CGM)}, \qquad \lambda^l = \frac{(\vec{r}^{\,l}, \mathbf{A}\vec{n}^{\,l})}{(\mathbf{A}\vec{n}^{\,l}, \mathbf{A}\vec{n}^{\,l})} \quad \text{(CRM)}. \tag{26}$$

For both methods, the updated residuals are determined using $\vec{n}^{\,l}$ and the corresponding λ^l

$$\vec{r}^{\,l+1} = \vec{r}^{\,l} - \lambda^l \mathbf{A}\vec{n}^{\,l}\,. \tag{27}$$

The vectors $\vec{n}^{\,l}$ are conjugate search directions in error space (directions are called conjugate when the minimization along one direction does not interfere with a minimization along another direction, i.e., if $\vec{n}^{\,k}\mathbf{A}\vec{n}^{\,l} = 0$, $k \neq l$). The search direction for the following iteration may be found as that part of the residual which is normal to all previous search directions leading to two different expressions for CGM and CRM

$$\vec{n}^{\,l+1} = \vec{r}^{\,l+1} + \kappa^l \vec{n}^{\,l} \quad \text{(CGM)}, \qquad \vec{n}^{\,l+1} = \vec{r}^{\,l+1} + \sum_{j=0}^{l} \kappa_j^l \vec{n}^{\,j} \quad \text{(CRM)}, \tag{28}$$

where the orthogonality coefficients are given as

$$\kappa^l = \frac{(\vec{r}^{\,l+1}, \vec{r}^{\,l+1})}{(\vec{r}^{\,l}, \vec{r}^{\,l})} \quad \text{(CGM)} \qquad \text{and} \qquad \kappa_j^l = \frac{(\mathbf{A}\vec{n}^{\,j}, \mathbf{A}\vec{r}^{\,l+1})}{(\mathbf{A}\vec{n}^{\,j}, \mathbf{A}\vec{n}^{\,j})} \quad \text{(CRM)}. \tag{29}$$

The above outlined sequence of vectors satisfies the conjugacy condition

$$\vec{n}^{\,k}\mathbf{A}\vec{n}^{\,l} = 0\,, \quad k \neq l\,, \tag{30}$$

as well as the orthogonality condition

$$(\vec{r}^{\,l}, \vec{r}^{\,k}) = 0\,, \quad k \neq l\,. \tag{31}$$

3.2 Preconditioning

The rate of convergence is related to the condition number of the matrix and the eigenspectrum of the matrix **A**. The rate of convergence of these methods may be accelerated by preconditioning of the matrix **A**, i.e., solving the equivalent system

$$(\mathbf{H}^{-1}\mathbf{A})\vec{x} = \mathbf{H}^{-1}\vec{b},$$

where $\mathbf{H}^{-1}$ is an approximate inverse of **A**, and $(\mathbf{H}^{-1}\mathbf{A}) \approx \mathbf{I}$. Note that the identity matrix **I** has a condition number of 1.

As an example we discuss the SSOR–preconditioning method according to Schwarz (1991), which goes back to the work of Evans (1968). The preconditioner has been applied to all of our tested equation solvers after scaling the matrix and was chosen because no additional storage for the preconditioning matrix is required. The symmetrized and scaled coefficient matrix **A** can be written as the sum of a lower triangular matrix **E**, an upper triangular matrix **F**, and the identity matrix **I**, respectively:

$$\mathbf{A} = \mathbf{E} + \mathbf{I} + \mathbf{F} \quad , \tag{32}$$

with $\mathbf{F} = \mathbf{E}^T$. The preconditioning matrix **H** is defined by

$$\mathbf{H} = \mathbf{C}\,\mathbf{C}^T \quad . \tag{33}$$

For **C** we choose a matrix similar to the above defined matrix **E**, giving **C** the nonzero pattern of the strictly lower part of **A**. Then, **H** reads as follows:

$$\mathbf{H} = (\mathbf{I} + \omega\mathbf{E})(\mathbf{I} + \omega\mathbf{F}) \tag{34}$$

where $\mathbf{C} = \mathbf{I} + \omega\mathbf{E}$, and $\omega \in I\!R$ denotes a relaxation factor. It is chosen to be $\omega = 1.4$ (eq. 34). When ω is plotted as a function of the convergence rate, it describes a broad minimum around the chosen value of 1.4. Numerous tests have confirmed, that this value ensures rapid convergence. Slight alterations of ω do not affect the relaxation process significantly. The unpreconditioned algorithm is obtained for $\omega = 0.0$

SSOR–preconditioning has the advantage of not requiring any further memory because the preconditioning matrix **H** is not explicitly constructed and stored. Incomplete factorization methods are usually efficient alternatives, although the preconditioning matrix requires additional storage. However, they may break down because of attempted division by zero pivot. Substituting the zero pivot by an arbitrary positive value avoids breakdown [e.g., incomplete Cholesky preconditioning (Kershaw 1978)]. Although factorization requires additional fpo's per equation and iteration, the total cumulative amount of numerical work is reduced by accelerating the convergence. A more detailed comparison of different preconditioners is subject to future investigations.

3.3 The Methods

3.3.1 Conjugate Gradients [CG]

CG (Hestenes & Stiefel 1952) uses 25 (39 with preconditioning) ×N fpo's per iteration, where N denotes the number of equations and the value in brackets is the respective number of iterations for the SSOR–preconditioned version. Storage requirements are 10 × N elements for the SSOR–preconditioned version. As stated above, CG is limited to symmetric matrices owing to the chosen functional to be minimized.

3.3.2 Bi–Conjugate Gradients [BICG]

For the solution of non-symmetric matrix equation systems ($\mathbf{A}^\mathbf{T} \neq \mathbf{A}$) the BICG method (Fletcher 1976) can be used. BICG uses 2 similar conjugate search direction vectors $\vec{n}$ and $\tilde{\vec{n}}$ resulting in two residual vectors $\vec{r}$ and $\tilde{\vec{r}}$. These quantities correspond to **A** and $\mathbf{A}^\mathbf{T}$. The update vector $\Delta\vec{x}$ is a function of both search direction vectors $\vec{n}$ and $\tilde{\vec{n}}$. BICG is more general than CG and includes CG for $\vec{r} = \tilde{\vec{r}}$ and $\vec{n} = \tilde{\vec{n}}$.

Compared to CG, the number of fpo's increases from 25 (39 with preconditioning) ×N to 42 (70 with preconditioning) ×N per iteration. Storage requirements are 14 × N elements.

3.3.3 Conjugate Gradients Squared [CGS]

CGS (Sonneveld 1989) is applicable for non–symmetric matrices and constitutes a variant of BICG, avoiding the use of the transpose $\mathbf{A}^T$. It is derived from a polynomial description of CG and BICG regarding the residual vector $\vec{r}_i$ as the product of $\vec{r}_0$ and an i^{th} degree polynomial in $\mathbf{A}$ termed $P_i(\mathbf{A})$: $\vec{r}_i = P_i(\mathbf{A})\,\vec{r}_0$. Satisfying also $\tilde{\vec{r}}_i = P_i(\mathbf{A}^T)\,\tilde{\vec{r}}_0$, we obtain

$$(\tilde{\vec{r}}_i, \vec{r}_i) = (P_i(\mathbf{A}^T)\,\tilde{\vec{r}}_0, P_i(\mathbf{A})\,\vec{r}_0) = (\tilde{\vec{r}}_0, P_i^2(\mathbf{A})\,\vec{r}_0) \quad . \tag{35}$$

The "contraction" operator $P_i(\mathbf{A})$ is applied twice on $\vec{r}_n$ instead of exploiting the quasi residuals $\tilde{\vec{r}}_n$ ($\rightarrow$ CG Squared). 45 (73 with preconditioning) fpo's per iteration and equation and 15 × N elements for storage are required.

3.3.4 Bi–Conjugate Gradients Stabilized [BICGSTAB]

BICGSTAB (Van der Vorst 1992) is a variant of CGS avoiding its unstable convergence behaviour. It is applicable on non–symmetric matrices without using the transpose $\mathbf{A}^T$. Instead of using the "contraction" operator twice $P_i^2(\mathbf{A})\,\vec{r}_0$, it computes a sequence $Q_i(\mathbf{A})\,P_i(\mathbf{A})\,\vec{r}_0$ using the polynomial Q_i as a description of a steepest descent update. BICGSTAB needs 48 (76 with preconditioning) fpo's per iteration and equation and 14 × N elements for storage.

3.3.5 Orthomin [ORTHOMIN]

The orthomin method (Behie and Vinsome 1982, Vinsome 1976) is a truncated conjugate residual method that is restarted every four or five iterations using a shift vector $\vec{v}$ to obtain a new search direction. The shift vector is defined as the solution of a residual equation.

$$\vec{v}^{\,l+1} = \mathbf{H}^{-1}\vec{r}^{\,l} \tag{36}$$

that incorporates the preconditioning step. The approximate inverse $\mathbf{H}^{-1}$ of $\mathbf{A}$ can be obtained using SSOR preconditioner. 51 (65 with preconditioning) fpo's per iteration and equation and 15 × N elements for storage are needed.

3.4 Summary of Storage Requirements and Floating Point Operations

Table 1 summarizes the storage requirements and fpo's per equation and iteration. Generalization to non-symmetric matrices and preconditioning generally add to the storage requirements and the number of fpo's per iteration and equation, respectively.

Method	fpo's	Storage	remarks
CG	25 (39) × N	10 × N	PDS matrices only
BICG	42 (70) × N	14 × N	
CGS	45 (73) × N	15 × N	
BICGSTAB	48 (76) × N	14 × N	
ORTHOMIN	51 (65) × N	15 × N	

Table 1: Comparison of floating point operations (fpo) per iteration and storage requirements. N denotes the number of equations, the value in brackets stands for the SSOR–preconditioned method.

3.5 Results

Fig. 9, 10, and 11 show the convergence behaviour of the preconditioned methods described above in terms of fpo's per equation for the homogeneous halfspace, the dike model, and the three–layered earth from section 2.2. The ordinate denotes the normalized residual $|\vec{r}_k|/|\vec{r}_0|$ with $|\vec{r}_0|$ as the residual for the starting value $\vec{x}_0$ and the abscissa indicates the number of fpo's. As an example Fig. 9 additionally displays the results of the unpreconditioned versions with the relaxation factor $\omega = 0$ (eq. 34). As is expected, they converge considerably slower. Therefore, and for reasons of clarity the other two diagrams

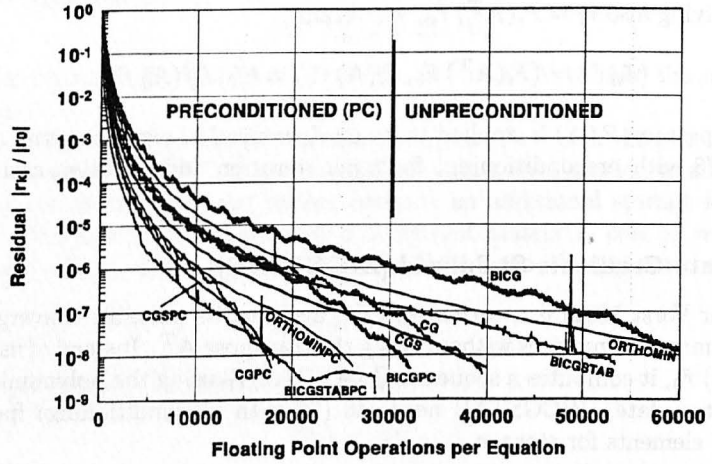

Figure 9: Comparison for a homogeneous halfspace.

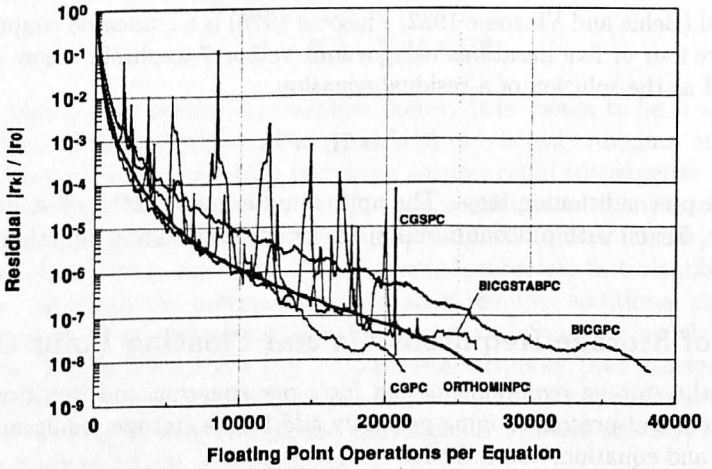

Figure 10: Comparison for a dike model.

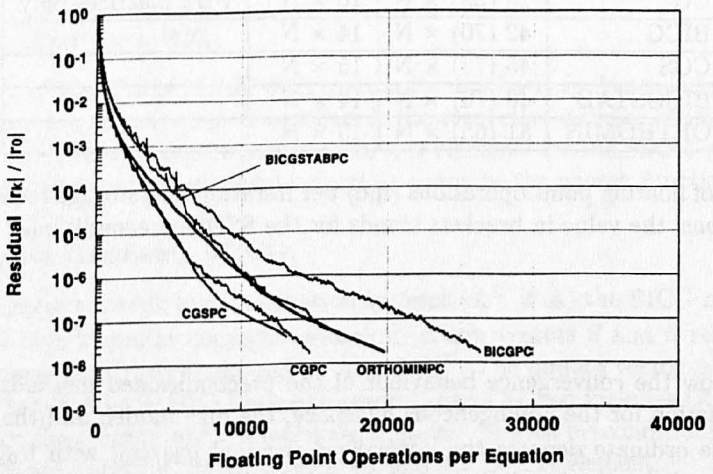

Figure 11: Comparison for a three–layered earth.

are restricted to the preconditioned methods (indicated by the extension ...PC). In future work, the efficiency of other preconditioners needs to be included in the comparison.

In all three cases, CGPC and CGSPC are among the fastest equation solvers, although CGSPC may show unstable behaviour (fig. 10). Also BICGSTABPC sometimes shows spikes (especially in fig. 9), but generally is relatively steady. The convergence behaviour of ORTHOMINPC is very smooth in each case. Finally BICGPC yields the slowest convergence rates for each of the investigated models.

4 Conclusions

The examples show that accuracy of modeling depends on the method of discretization. It is demonstrated that three (BT&W, D&M2, ZM&M) of the five discretization methods yield accurate results especially when conductivity contrasts (e.g., dikes, layers) are introduced into the halfspace. For four of the five methods (BT&W, D&M1, D&M2, W&M), the spatial discretization is the same while the discretzation and method of averaging conductivities differ. The accuracy of these methods clearly depends on the method of discretizing conductivities. ZM&M's approach cannot be decomposed into spatial and conductivity discretization.

The speed of convergence of the equation solvers depends on the selected conjugate gradient/residual method as well as on preconditioning. Therefore, preconditioning is highly recommended to improve convergence. The preconditioned conjugate gradient method (CGPC) and the preconditioned conjugate gradients squared (CGSPC) generally show the fastest convergence. BICGSTAB and ORTHOMIN achieve good convergence but they are somewhat slower than CGPC an CGSPC. The smoothest convergence behaviour is shown by ORTHOMIN indicating robustness and stability. However, CGPC is only applicable for symmetric matrices. The spikes in the convergence behaviour of CGSPC and BICGSTAB may indicate that the algorithms can fail to converge. In conclusion, we recommend CGPC for symmetric matrices and ORTHOMIN as a more general equation solver.

Acknowledgments

We would like to acknowledge valuable discussions with A. Mezzatesta, M. Rabinovich, T. Tamarchenko (all at Western Atlas Logging Services, Houston), R.A. Wattenbarger (Texas A&M University), R. Schulz and H. Rodemann (both at Niedersächsisches Landesamt für Bodenforschung – Geowissenschaftliche Gemeinschaftsaufgaben, Hannover).

References

Agarwal, A.K. & Weaver, J.T., 1994. A parallel implementation of conjugate gradient methods over a network of UNIX-based workstations, *abstract proceedings of 12th EM Induction workshop*, held in Brest, France, during August 8–13, p82.

Behie, A., & Vinsome, P.K.W., 1982. Block iterative methods for fully implicit reservoir simulation, *SPE Journal*, **22**, 658 – 668.

Brewitt–Taylor, C.R., & Weaver, J.T., 1976. On the finite difference solution of two–dimensional induction problems, *Geophys. J. R. astr. Soc.*, **47**, 375 – 396.

Dey, A., & Morrison, H.F., 1979a. Resistivity modelling for arbitrarily shaped two–dimensional structures, *Geophys. Prosp.*, **27**, 106 – 136.

Dey, A., & Morrison, H.F., 1979b. Resistivity modelling for arbitrarily shaped three–dimensional structures, *Geophysics*, **44**, 753 – 780.

Evans, D.J., 1968. The use of preconditioning in iterative methods for solving linear equations with symmetric positive definite matrices, *J. Inst. Maths. Applics.*, **4**, 295 – 314.

Fletcher, R., 1976. Conjugate gradient methods for indefinite systems, *Lecture Notes in Mathematics*, **506**, 73 – 89.

Hestenes, M.R., & Stiefel, E., 1952. Method of conjugate gradients for solving linear systems, *J. Res. Nat. Bur. Standards*, **49**, 409 – 436.

Kershaw, D.S., 1978. The incomplete Cholesky-conjugate gradient method for the iterative solution of systems of linear equations, *J. Comput. Phys.*, **26**, 43 – 65.

Koefoed, O., 1979. *Geosounding principles 1.*, Elsevier, Amsterdam – Oxford – New York.

Madden, T.R., 1972. Transmission systems and network analogies to geophysical forward and inverse problems, Report No. **72-3**, Dept. of Earth and Planetary Sciences, M.I.T., Cambridge, Massachusetts, USA.

Mundry, E., 1984. Geoelectrical model calculations for two–dimensional resistivity distributions, *Geophys. Prosp.*, **32**, 124 – 131.

Press, W.H., Flannery, B.P., Teukolsky, S.A., and Vetterling, W.T., 1989. Numerical recipes, Cambridge University Press.

Rodemann, H., 1994. Einige Diskretisierungs–Effekte bei Modellrechnungen zur Geoelektrik nach der Methode der finiten Differenzen, in Bahr, K. & Junge, A. (eds.), Protokoll 15. Kolloquium "Elektromagnetische Tiefenforschung" in Höchst/Odenwald, 200 – 203.

Rossen, R.H. & Dalton, R.L., 1990. Selecting grid and timestep sizes, in *Reservoir Simulation*, ed. Mattox, C.C. & Dalton, R.L., SPE Monograph **13**, 44-56.

Schwarz, H.R., 1991. *Methode der finiten Elemente*, Teubner, Stuttgart.

Scriba, H., 1981. Computation of the electric potential in three–dimensional structures, *Geophys. Prosp.*, **29**, 790 – 802.

Sonneveld, P., 1989. CGS: a fast Lanczos–type solver for nonsymmetric linear systems, *SIAM J. Sci. Statist. Comput.*, **10**, 36 – 52.

Spitzer, K., 1995. A 3D finite difference algorithm for DC resistivity modeling using conjugate gradient methods, *Geophys. J. Int.*, **123**, 903 – 914.

Telford, W.M., Geldart, L.P., & Sheriff, R.E., 1990. *Applied Geophysics*, 2nd ed., Cambridge University Press, Cambridge.

Vinsome, P.K.W., 1976. Orthomin, an iterative method for solving sparse sets of simultaneous linear equations, Society of Petroleum Engineers of AIME, Paper SPE 5729, 149 – 159.

Van der Vorst, H., 1992. Bi–CGSTAB: A fast and smoothly converging variant of Bi–CG for the solution of nonsymmetric linear systems, SIAM J. Sci. Statist. Comput., **13**, 631 – 644.

Wurmstich, B., & Morgan, F.D., 1994. Modeling of streaming potential responses caused by oil well pumping, *Geophysics*, **59**, 46 – 56.

Zhang, J., Mackie, R.L., & Madden, T.R., 1995. 3-D resistivity forward modeling and inversion using conjugate gradients, *Geophysics*, **60**, 1313 – 1325.